Inorganic Chemistry

Article

pubs.acs.org/IC

Synthesis, Structure, and Characterization of Two New Polar Sodium Tungsten Selenites: $Na_2(WO_3)_3(SeO_3)\cdot 2H_2O$ and $Na_6(W_6O_{19})(SeO_3)_2$

Sau Doan Nguyen and P. Shiv Halasyamani*

Department of Chemistry, University of Houston, 136 Fleming Building, Houston, Texas 77204-5003, United States

Supporting Information

ABSTRACT: Two new quaternary sodium tungsten selenites, $Na_2(WO_3)_3(SeO_3)\cdot 2H_2O$ ($P3_1c$) and $Na_6(W_6O_{19})(SeO_3)_2$ ($C2$), have been synthesized and characterized. The former exhibits a hexagonal tungsten oxide layered structure, whereas the latter has a one-dimensional "ribbon" structure. The layers and "ribbons" consist of distorted WO_6 and asymmetric SeO_3 polyhedra. The layers in $Na_2(WO_3)_3(SeO_3)\cdot 2H_2O$ and the "ribbons" in $Na_6(W_6O_{19})(SeO_3)_2$ are separated by Na^+ cations. Powder second-harmonic-generation (SHG) measurements on $Na_2(WO_3)_3(SeO_3)\cdot 2H_2O$ and $Na_6(W_6O_{19})(SeO_3)_2$ using 1064 nm radiation reveal SHG efficiencies of approximately 450× and 20× α-SiO_2, respectively. Particle size versus SHG efficiency measurements indicate that the materials are type 1 non-phase-matchable. Converse piezoelectric measurements result in d_{33} values of approximately 23 and 12 pm/V, whereas pyroelectric measurements reveal coefficients of −0.41 and −1.10 $\mu C/m^2\cdot K$ at 60 °C for $Na_2(WO_3)_3(SeO_3)\cdot 2H_2O$ and $Na_6(W_6O_{19})(SeO_3)_2$, respectively. Frequency-dependent polarization measurements confirm that the materials are nonferroelectric; i.e., the macroscopic polarization is not reversible, or "switchable". IR and UV−vis spectroscopy, thermogravimetric and differential thermal analysis measurements, and electron localization function calculations were also done for the materials. Crystal data: $Na_2(WO_3)_3(SeO_3)\cdot 2H_2O$, trigonal, space group $P3_1c$ (No. 159), a = 7.2595(6) Å, b = 7.2595(6) Å, c = 12.4867(13) Å, V = 569.89(9) $Å^3$, Z = 2; $Na_6(W_6O_{19})(SeO_3)_2$, monoclinic, space group $C2$ (No. 5), a = 42.169(8) Å, b = 7.2690(15) Å, c = 6.7494(13) Å, β = 98.48(3)°, V = 2046.2(7) $Å^3$, Z = 4.

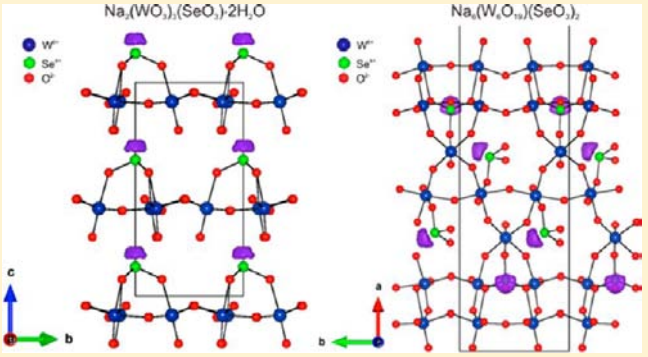

INTRODUCTION

Polar materials, which crystallize in 1 of 10 polar crystal classes (1, 2, 3, 4, 6, m, 3m, 2mm, 4mm, and 6mm), exhibit technologically functional properties like second harmonic generation (SHG), piezoelectricity, pyroelectricity, and/or ferroelectricity.[1−8] The synthetic exploration and crystal engineering of new polar materials continue to be an active and challenging task for material scientists and solid-state chemists. The crystal engineering of polar materials studies the design and packing of polar structural units. Molecules with organic π-conjugated systems, typically nitropyridine oxide, alkali-metal acid phthalate, or nitroaniline families, are widely used as polar structural units in preparing new nonlinear-optical (NLO) organic crystals.[9,10] Chen's anionic group theory proposed using acentric inorganic π-conjugated systems, particularly planar borate rings, to enhance NLO responses of noncentrosymmetric (NCS) borate-based materials.[11−14] Recently, Zou et al. have successfully reported a new series of polar alkaline−alkaline-earth fluoride carbonates with strong SHG efficiencies based on π-conjugated CO_3^{2-} anions.[15] Poeppelmeier and co-workers have successfully used oxyfluoride groups to create new polar materials,[16−20] whereas cations that are susceptible to second-order Jahn−Teller (SOJT) distortions[21−27] have been successfully employed in preparing many new polar materials in our group, as well as other research groups.[28−38]

While polar structural units can be successfully and specifically designed for preparing new polar materials, the understanding of how polar structures are created from structural building units is insufficient. The packing and alignments of polar structural units strongly depend on intermolecular interactions, i.e., cation−anion interactions and hydrogen bonding. Hydrogen bonding has been widely used in NLO organic crystal engineering to obtain a designed crystal packing[39−45] but less obviously employed in preparing polar inorganic materials. The strong hydrogen bonds, O−H···O and N−H···O, formed along the lone-pair directions arrange the organic molecules into polar three-dimensional networks, and the crystal structures are additionally stabilized via weaker C−H···O hydrogen bonds. A systematic review of hydrogen bonding in inorganic materials and its influence on the NLO properties of polar materials has recently been published.[46] Recently, using hydrogen bonding to direct the alignment of polar λ structural building units, Donakowski et al. have been able to prepare a new polar material, $CuVOF_4(H_2O)_7$, from

Received: December 5, 2012
Published: February 20, 2013

   dx.doi.org/10.1021/ic3026705 | Inorg. Chem. 2013, 52, 2637−2647

centrosymmetric (CS) $MVOF_4(H_2O)_7$ (M = Co^{2+}, Ni^{2+}, and Zn^{2+}).[20] However, hydrogen bonds in preparing new NCS oxide materials have not been extensively explored. The influence of cation sizes on altering the packing and alignments of polar structural units has been observed and reported for several systems such as $MNaNbOF_5$ (M = K^+ and Cs^+),[19] $A_2Ti(IO_3)_6$ (A = Li^+, Na^+, K^+, Rb^+, Cs^+, and Tl^+),[47] $ACuTe_2O_7$,[48] and $A(Mo_2O_5)(SeO_3)_2$ (A = Sr^{2+}, Ba^{2+}, and Pb^{2+}).[49] Recently, using hard, Na^+, and soft, Ag^+, cations, Fry et al. have been able to direct the orientation of polar oxyfluoride groups, thereby altering the undoped polar $Na_3WO_3F_3$ ($R3$) to the doped CS $Na_{1.5}Ag_{1.5}MoO_3F_3$ and $Na_{1.5}Ag_{1.5}WO_3F_3$ ($R\bar{3}$).[50] Despite these successes, the systematic engineering and design of new polar crystal structures remain an ongoing challenge.

With respect to sodium compounds containing SOJT cations, many sodium d^0 tellurites, $NaTeVO_5$ ($P2_1/c$),[51,52] $Na_2MTe_4O_{12}$ (M = Mo^{6+} and W^{6+}; $C2/c$),[53] $Na_2Mo_3Te_3O_{16}$ ($I2$),[31] and $Na_2TeW_2O_9$ (Ia),[54] were reported, whereas for sodium d^0 selenites, only Na_2SeMoO_6 ($P2_13$)[55] was found. In this paper, we report on the synthesis and characterization of two new polar sodium−tungsten selenites: $Na_2(WO_3)_3(SeO_3)\cdot 2H_2O$ ($P3_1c$) and $Na_6(W_6O_{19})(SeO_3)_2$ ($C2$). The former has a class 2 hexagonal tungsten oxide (HTO)-layered structure, i.e., the SeO_3 group "cap" on one side of the HTO layer,[56] and the latter has a one-dimensional "ribbon" structure. In addition to the crystal structures, UV−vis and IR spectroscopy, thermal analyses, and SHG, piezoelectricity, and polarization measurements for all materials are also reported.

EXPERIMENTAL DETAILS

Reagents. Na_2CO_3 (Alfa Aesar, 99%), SeO_2 (Alfa Aesar, 99.4%), $Na_2WO_4\cdot 2H_2O$ (Alfa Aesar, 99%), and WO_3 (Alfa Aesar, 99.8%) were used as received.

Synthesis. Crystals of polycrystalline $Na_2(WO_3)_3(SeO_3)\cdot 2H_2O$ were prepared using hydrothermal techniques. A 23 mL Teflon-lined autoclave containing 0.159 (1.50×10^{-3} mol) of Na_2CO_3, 0.174 g (7.50×10^{-4} mol) of WO_3, 0.330 g (3.00×10^{-3} mol) of SeO_2, 0.117 g (2.00×10^{-3} mol) of NaCl, and 2 mL of distilled water was closed, heated to 230 °C, held for 2 weeks, and cooled slowly to room temperature at a rate of 6 °C/h. The product was filtered and washed three times with distilled water to obtain 0.137 g of tiny yellow hexagonal plate-shaped crystals (in 60% yield with respect to WO_3). The crystals were structurally determined as $Na_2(WO_3)_3(SeO_3)\cdot 2H_2O$. The experimental and calculated powder X-ray diffraction (PXRD) data for $Na_2(WO_3)_3(SeO_3)\cdot 2H_2O$ are provided in the Supporting Information (see Figure S1).

Crystals of $Na_6(W_6O_{19})(SeO_3)_2$ were prepared by solid-state techniques. A mixture of 0.106 (1.00×10^{-3} mol) of Na_2CO_3, 0.232 g (1.00×10^{-3} mol) of WO_3, and 0.110 g (1.00×10^{-3} mol) of SeO_2 was ground and pressed into a pellet. The pellet was transferred to a Pyrex tube, and the tube was heated at 300 °C for 1 day. The thermal analysis of the pellet after heating at 300 °C shows that all CO_2 was removed (see Figure S4 in the Supporting Information). The tube was then air-evacuated and flame-sealed to an ampule. The ampule was then heated to 450 °C for 2 days and cooled slowly to room temperature at a rate of 6 °C/h. The pellet was then washed with distilled water and revealed colorless rod-shaped crystals. The crystals were later structurally determined to be $Na_6(W_6O_{19})(SeO_3)_2$.

Polycrystalline $Na_6(W_6O_{19})(SeO_3)_2$ was prepared by combining 0.990 g (3.00×10^{-3} mol) of $Na_2WO_4\cdot 2H_2O$, 0.700 g (3.00×10^{-3} mol) of WO_3, and 0.220 g (2.00×10^{-3} mol) of SeO_2. The mixture was finely ground and pressed into a pellet. The pellet was transferred to a Pyrex tube, and the tube was air-evacuated at 110 °C for 1 day and then flame-sealed to an ampule. The ampule was then heated to 450 °C for 2 days and finally 550 °C for 2 days with three intermittent regrindings, resulting in single-phase $Na_6(W_6O_{19})(SeO_3)_2$. The experimental and calculated PXRD data for $Na_6(W_6O_{19})(SeO_3)_2$ are provided in the Supporting Information (see Figure S1).

Single-Crystal X-ray Diffraction. For $Na_2(WO_3)_3(SeO_3)\cdot 2H_2O$, a yellow plate-shaped crystal ($0.01 \times 0.01 \times 0.002$ mm^3) and for $Na_6(W_6O_{19})(SeO_3)_2$ a colorless rod-shaped crystal ($0.04 \times 0.01 \times 0.01$ mm^3) were used for single-crystal X-ray data collections. Data were collected using a Siemens SMART APEX diffractometer equipped with a 1 K CCD area detector using graphite-monochromated Mo Kα radiation. A hemisphere of data was collected using a narrow-frame method with scan widths of 0.30° in ω and an exposure time of 60 s/frame. The first 50 frames were remeasured at the end of the data collection to monitor the instrument and crystal stability. The data were integrated using the Siemens *SAINT* program,[57] with the intensities corrected for Lorentz, polarization, air absorption, and absorption attributable to the variation in the path length through the detector face plate. ψ scans were used for absorption correction on the hemisphere of data.[58] The data were solved and refined using *SHELXS-97* and *SHELXL-97*, respectively.[59,60] All of the atoms were refined with anisotropic thermal parameters, and the refinement converged for $I > 2\sigma(I)$. All calculations were performed using the *WinGX-98* crystallographic software package.[61] Crystal data of $Na_2(WO_3)_3(SeO_3)\cdot 2H_2O$ were checked for merohedral twinning using the *ROTAX* tool in the *WinGX-98* package.[61] During the refinement of $Na_2(WO_3)_3(SeO_3)\cdot 2H_2O$, the twin law −1 0 0 0 −1 0 0 0 1 suggested by *ROTAX* was successfully applied. Pseudomerohedral twinning was consistent with the refined BASF value of 0.26. The twin law indicates that the twinning lattices are related by a 180° rotation about the [001] direct lattice direction, the C3 rotation axis in the trigonal system that emulates higher hexagonal symmetry. In fact, when ADDSYM was run on the final model of $Na_2(WO_3)_3(SeO_3)\cdot 2H_2O$, higher hexagonal symmetry was suggested. Attempts to refine the obtained $Na_2(WO_3)_3(SeO_3)\cdot 2H_2O$ model in hexagonal space groups ($P6_3mc$) failed because Se atoms, which are located on the Wyckoff 2a site, will form planar SeO_3 equilateral triangles as required by the mirror symmetry of that Wyckoff site. Partial occupancy was observed for the Na atom on the 6c site. The occupancy was set to 0.6667. H-atom positions were not determined for $Na_2(WO_3)_3(SeO_3)\cdot 2H_2O$, and the thermal ellipsoids of the O atoms [O(5) and O(6)] of the H_2O molecule are comparatively large compared with the other ions. However, the H_2O molecules were experimentally confirmed by the IR spectrum and thermogravimetric analysis (TGA). Merohedral twinning (type 1, inversion twinning) was observed for $Na_6(W_6O_{19})(SeO_3)_2$; thus, a twin law −1 0 0 0 −1 0 0 0 −1 was applied. This inversion twinning in combination with a 2-fold rotation along the b axis results in a pseudomirror plane. This mirror plane was detected by ADDSYM; however, the ADDSYM EXACT calculation confirmed $C2$ to be the correct space group. Additionally, refinement of $Na_6(W_6O_{19})(SeO_3)_2$ in space group Cm results in numerous atoms on the Wyckoff 2a site with mirror symmetry, and no chemically reasonable structure could be obtained. The Flack parameters[62] were refined to 0.01(5) and 0.00(10) for $Na_2(WO_3)_3(SeO_3)\cdot 2H_2O$ and $Na_6(W_6O_{19})(SeO_3)_2$, respectively. Crystallographic data and selected bond distances for $Na_2(WO_3)_3(SeO_3)\cdot 2H_2O$ and $Na_6(W_6O_{19})(SeO_3)_2$ are given in Tables 1 and 2.

PXRD. The PXRD data for all materials were collected in a continuous mode using a PANalytical X'Pert PRO diffractometer at room temperature (Cu Kα radiation, flat-plate geometry) equipped with an X'Celerator detector. Data were collected in the 2θ range of 5−70° with a step size of 0.016° and a step time of 10 s.

IR Spectroscopy. IR spectra were recorded on a Matteson FTIR 5000 spectrometer in the spectral range of 400−4000 cm^{-1} at room temperature. $Na_2(WO_3)_3(SeO_3)\cdot 2H_2O$ and $Na_6(W_6O_{19})(SeO_3)_2$ powders were heated to 150 °C for 1 week before being mixed and ground with dry KBr powder. These powder mixtures were then transferred to a stainless steel IR holder and pressed into semi-transparent pellets, which were used for IR measurements.

dx.doi.org/10.1021/ic3026705 | *Inorg. Chem.* 2013, 52, 2637−2647

Table 1. Crystallographic Data for $Na_2(WO_3)_3(SeO_3)\cdot 2H_2O$ and $Na_6(W_6O_{19})(SeO_3)_2$

	$Na_2(WO_3)_3(SeO_3)\cdot 2H_2O$	$Na_6(W_6O_{19})(SeO_3)_2$
fw (g/mol)	904.49	1798.96
T (K)	298.0(2)	298.0(2)
λ (Å)	0.71073	0.71073
cryst syst	trigonal	monoclinic
space group	$P3_1c$ (No. 159)	$C2$ (No. 5)
a (Å)	7.2595(6)	42.169(8)
b (Å)	7.2595(6)	7.2690(15)
c (Å)	12.4867(13)	6.7494(13)
α (deg)	90	90
β (deg)	90	98.48(3)
γ (deg)	120	90
V (Å^3)	569.89(9)	2046.2(7)
Z	2	4
ρ_{calcd} (g/cm^3)	5.248	5.840
μ (mm^{-1})	33.549	37.401
R(int)	0.0671	0.0412
GOF (F^2)	1.030	1.064
$R(F)^a$	0.0391	0.0331
$R_w(F_o^2)^b$	0.0870	0.0895
Flack parameter	0.01(5)	0.00(10)

$^aR(F) = \sum||F_o| - |F_c||/\sum|F_o|$. $^bR_w(F_o^2) = [\sum w(F_o^2 - F_c^2)^2/\sum w(F_o^2)^2]^{1/2}$.

UV–Vis Diffuse-Reflectance Spectroscopy. UV–vis diffuse-reflectance spectra were collected with a Varian Cary 500 scan UV–vis–near-IR spectrophotometer over the spectral range of 200–2000 nm at room temperature. Poly(tetrafluoroethylene) (PTFE) was used as a standard material for baseline correction. The sample was thoroughly mixed with PTFE, and this mixture was used for UV–vis measurements. Reflectance spectra were converted to absorbance using the Kubelka–Munk equation.[63,64]

Thermal Analysis. Thermogravimetric (TGA) and differential thermal (DTA) analyses were simultaneously carried out on an EXSTAR6000 TG/DTA 6300 thermogravimetric/differential thermal analysis system (SII NanoTechnology Inc.). The sample (~20 mg) was placed in a platinum crucible, which was heated (cooled) at a rate of 10 °C/min in the range of 25–700 °C under flowing nitrogen gas. An empty platinum crucible was used as the reference during the measurements.

SHG. The powder SHG measurements of $Na_2(WO_3)_3(SeO_3)\cdot 2H_2O$ and $Na_6(W_6O_{19})(SeO_3)_2$ were performed at room temperature on a modified Kurtz NLO system,[65] using a pulsed Nd:YAG laser with a wavelength of 1064 nm. The methodology and instrumentation details have been published.[66] The SHG efficiency has been shown to be particle-size-dependent.[65] Thus, the polycrystalline samples were ground and sieved into distinct particle size ranges (20–45, 45–63, 63–75, 75–90, and 90–120 μm). In order to evaluate the relative SHG efficiencies of the measured samples with known SHG materials, crystalline α-SiO_2 was also ground and sieved into the same particle size ranges. No index matching fluid was used in the experiment.

Piezoelectric Measurements. Converse piezoelectric measurements were performed at room temperature using a Radiant Technologies RT66A piezoelectric test system with a TREK (model 609E-6) high-voltage amplifier, Precision Materials Analyzer, Precision High Voltage Interface, and MTI 2000 Fotonic Sensor. $Na_2(WO_3)_3(SeO_3)\cdot 2H_2O$ and $Na_6(W_6O_{19})(SeO_3)_2$ samples were pressed into a pellet with approximately 8 mm diameter and approximately 1 mm thicknes. The pellets were sintered in air at 200 °C for $Na_2(WO_3)_3(SeO_3)\cdot 2H_2O$ or 300 °C for $Na_6(W_6O_{19})(SeO_3)_2$ for 1 week. Silver paste was applied to both sides of the sintered pellets as electrodes, and the pellets were cured in air at 200 °C for $Na_2(WO_3)_3(SeO_3)\cdot 2H_2O$ or 300 °C for $Na_6(W_6O_{19})(SeO_3)_2$ for 72 h. These pellets were also used in polarization measurements.

Polarization Measurements. The polarization measurements were done on a Radiant Technologies model RT66A ferroelectric test system with a TREK high-voltage amplifier in the temperature range of 25–160 °C in a Delta model 9023 environmental test chamber. The unclamped pyroelectric coefficient, defined as dP/dT,[66] was determined by measuring the polarization as a function of the

Table 2. Selected Bond Distances (Å) for $Na_2(WO_3)_3(SeO_3)\cdot 2H_2O$ and $Na_6(W_6O_{19})(SeO_3)_2$

$Na_2(WO_3)_3(SeO_3)\cdot 2H_2O^a$					
W(1)–O(1)	1.728(12)	W(1)–O(3)	1.863(13)	Se(1)–O(4)	3 × 1.703(12)
W(1)–O(2)	1.835(12)	W(1)–O(3)#2	2.051(13)		
W(1)–O(2)#1	1.998(12)	W(1)–O(4)	2.187(11)		
$Na_6(W_6O_{19})(SeO_3)_2^a$					
W(1)–O(1)	1.702(9)	W(4)–O(17)	1.731(10)	Se(1)–O(14)	1.680(8)
W(1)–O(2)	1.851(9)	W(4)–O(13)	1.735(11)	Se(1)–O(11)	1.748(9)
W(1)–O(3)	1.942(11)	W(4)–O(7)	1.932(11)	Se(1)–O(6)	1.750(9)
W(1)–O(4)	1.947(11)	W(4)–O(9)	1.943(11)	Se(2)–O(23)	1.658(10)
W(1)–O(5)	1.971(10)	W(4)–O(15)	2.176(9)	Se(2)–O(18)	1.660(11)
W(1)–O(6)	2.274(10)	W(4)–O(11)	2.347(10)	Se(2)–O(25)	1.765(10)
W(2)–O(10)	1.722(10)	W(5)–O(12)	1.730(9)		
W(2)–O(19)	1.753(10)	W(5)–O(5)	1.857(10)		
W(2)–O(9)	1.933(11)	W(5)–O(22)	1.877(9)		
W(2)–O(7)	1.935(11)	W(5)–O(24)	1.902(9)		
W(2)–O(2)	2.135(10)	W(5)–O(20)	1.954(10)		
W(2)–O(6)	2.366(10)	W(5)–O(14)	2.309(9)		
W(3)–O(16)	1.724(10)	W(6)–O(8)	1.739(9)		
W(3)–O(15)	1.830(9)	W(6)–O(20)	1.885(10)		
W(3)–O(3)	1.874(11)	W(6)–O(21)#3	1.915(9)		
W(3)–O(4)	1.969(10)	W(6)–O(21)	1.928(9)		
W(3)–O(22)	1.972(10)	W(6)–O(24)	1.951(9)		
W(3)–O(11)	2.273(10)	W(6)–O(25)	2.122(11)		

^{a}Symmetry transformations used to generate equivalent atoms: #1, $-x + y + 2, -x + 1, z$; #2, $-y + 1, x - y, z$; #3, $-x + {}^1/_2, y + {}^1/_2, -z + 1$.

dx.doi.org/10.1021/ic3026705 | Inorg. Chem. 2013, 52, 2637–2647

temperature. The methodology and instrumentation details have been published.[66] To measure the potential ferroelectric behavior, frequency-dependent polarization measurements were done at room temperature under a static electric field of 5 kV/cm between 100 and 1000 Hz. For the pyroelectric measurements, the polarization was measured statically from room temperature to 140 °C with an electric field of 5 kV/cm at 1000 Hz for $Na_2(WO_3)_3(SeO_3)\cdot 2H_2O$ and from room temperature to 160 °C with an electric field of 20 kV/cm at 100 Hz for $Na_6(W_6O_{19})(SeO_3)_2$. The temperature was allowed to stabilize before the polarization was measured.

Electron Localization Function (ELF) Calculations. ELF[67,68] calculations were performed using the plane-wave pseudopotential method, as implemented in the Quantum *ESPRESSO* (4.1.2 version)[69] package. Norm-conserving MT pseudopotentials for all of the elements were used with the generalized gradient approximation[70] for exchange-correlation corrections. The pseudopotentials generated from the Fritz Haber Institute code[71] were converted for the calculations. The tungsten pseudopotential was generated using previously reported parameters[72] by the *LD1* program. A plane-wave energy cutoff was set to 37 Ry. The Brillouin zone was sampled using a 4 × 4 × 3 Monkhorst–Pack[73] *k*-mesh. A total energy convergence threshold set to 10^{-6} Ry indicated self-consistency. The experimental crystal structures were employed for all calculations. The program *VESTA* was used for all of the structural diagrams.[74]

RESULTS AND DISCUSSION

Crystal Structures. $Na_2(WO_3)_3(SeO_3)\cdot 2H_2O$ crystallizes in NCS polar trigonal space group $P3_1c$. Ball-and-stick and polyhedra representations of the material in the (110) plane are shown in parts a and b of Figure 1. The material exhibits a HTO-layered structure with distorted WO_6 and asymmetric SeO_3 polyhedra (see Figure 2). Specifically, each WO_6 octahedron shares four equatorial O atoms with the other four WO_6 octahedra, thus forming a planar HTO layer with triangular and six-point star-ring holes. Regarding the connectivity of the AO_3 groups (A = Se^{4+} and Te^{4+}), the HTO layers can be further classified into two classes. Class 1 HTO layers consist of AO_3 groups (A = Se^{4+} and Te^{4+}) alternatively "capping" on triangular holes of both sides of the HTO layers, whereas in class 2 HTO layers, AO_3 groups (A = Se^{4+} and Te^{4+}) "cap" on the triangular holes on one side of the HTO layer.[56] In $Na_2(WO_3)_3(SeO_3)\cdot 2H_2O$, the SeO_3 polyhedra "cap" on the triangular holes of one side of the HTO layer, thus forming a class 2 HTO-layered structure. The layers stack on top of each other along the *c*-axis direction and are separated by Na^+ cations and the H_2O molecules. In connectivity terms, the structure may be written as $[3(WO_{1/1}O_{5/2})^-(SeO_{3/2})^+\cdot 2H_2O]^{2-}$ with charge balance maintained by two Na^+ cations. The W^{6+} cations are octahedrally coordinated to six O atoms with one "short" [1.728(12) Å], four "normal" [1.835(12)–2.015(13) Å], and one "long" [2.187(11) Å] W–O bonds. The "short" W–O bonds are terminal, and as expected, the W^{6+} cations displace toward terminal O atoms, i.e., a corner, C_4-type distortion, whereas the "long" W–O bonds are connected to SeO_3 groups. The Se^{4+} cations are in trigonal-pyramidal environments, coordinated to three O atoms with the same Se–O bond distance [1.703(12) Å]. Of the six O atoms in the asymmetric unit cell, O(5) and O(6) are isolated and have no bond to the W^{6+} and Se^{4+} cations. Therefore, O(5) and O(6) are O atoms of two H_2O molecules in $Na_2(WO_3)_3(SeO_3)\cdot 2H_2O$. The Na^+ cations are observed in seven-coordinated environments, bonded to two O atoms of the H_2O molecules with "short" Na–O bond distances [2.25(2)–2.47(4) Å] and to five O atoms of the WO_6 and SeO_3 polyhedra with "long" Na–O bond distances [2.44(2)–2.61(2) Å]. The experimental bond valence sums (BVSs in valence units, vu)[75] for the Na^+, W^{6+}, and Se^{4+} cations and O^{2-} anions, except for O(5) and (O6), are 1.16, 6.17, 3.96, and 2.01–2.07, respectively.

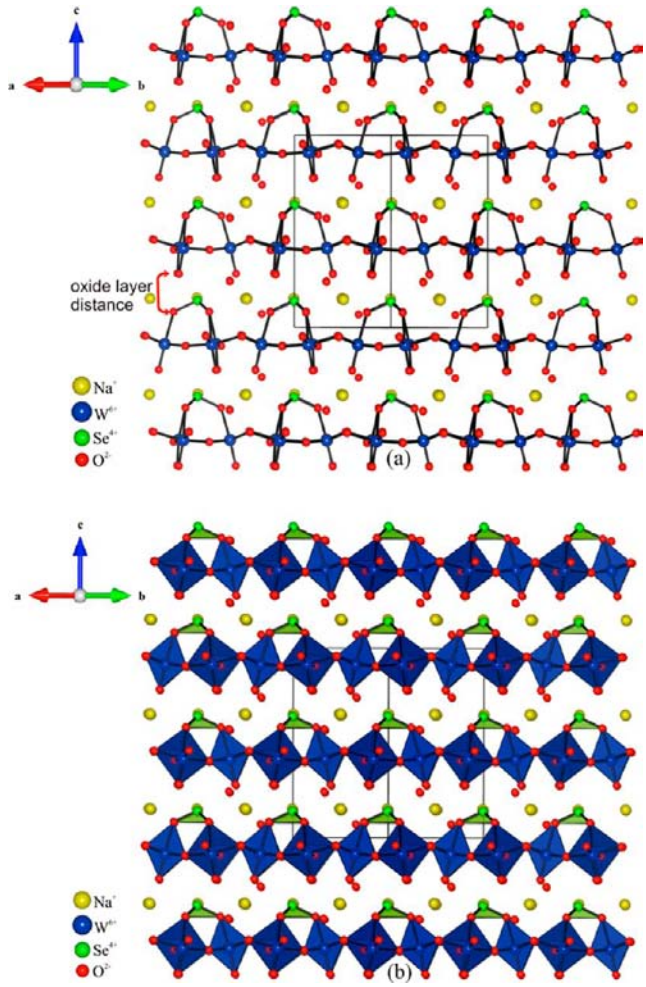

Figure 1. Ball-and-stick (top) and polyhedra (bottom) representations of $Na_2(WO_3)_3(SeO_3)\cdot 2H_2O$ in the (110) plane. Spheres in the diagram are Na^+ cations (yellow), W^{6+} cations (blue), Se^{4+} cations (green), and O^{2-} anions (red). Isolated red spheres are the H_2O molecules.

$Na_6(W_6O_{19})(SeO_3)_2$ crystallizes in NCS polar monoclinic space group *C*2. Ball-and-stick and polyhedra representations of the material in the *ac* plane are shown in parts a and b of Figure 3. The material exhibits an infinitive one-dimensional "ribbon" structure with distorted WO_6 and asymmetric SeO_3 polyhedra (see Figure 4). Specifically, $W(1)O_6$ and $W(2)O_6$ octahedra [similarly $W(3)O_6$ and $W(4)O_6$ octahedra] share an edge to form W_2O_{10} dimers. The W_2O_{10} dimers use apical O atoms to connect and form a "double chain" along the *b*-axis direction. Along the *b*-axis direction, the $W(6)O_6$ octahedra share apical O atoms to form a "single chain" between two "double chains". Two "double chains" and a "single chain" run in a parallel manner along the *b*-axis direction and are bridged by $W(5)O_6$ octahedra. The $W(5)O_6$ octahedra use four equatorial O atoms to connect the "double chain" to the "single chain", resulting in a "ribbon" structure. SeO_3 polyhedra attach to the "ribbon" in two different ways. $Se(1)O_3$ polyhedra "cap" on triangular holes formed by the "double chain" and $W(5)O_6$ octahedra, whereas $Se(2)O_3$ polyhedra are single-bonded to the "single chain" and

dx.doi.org/10.1021/ic3026705 | *Inorg. Chem.* 2013, 52, 2637–2647

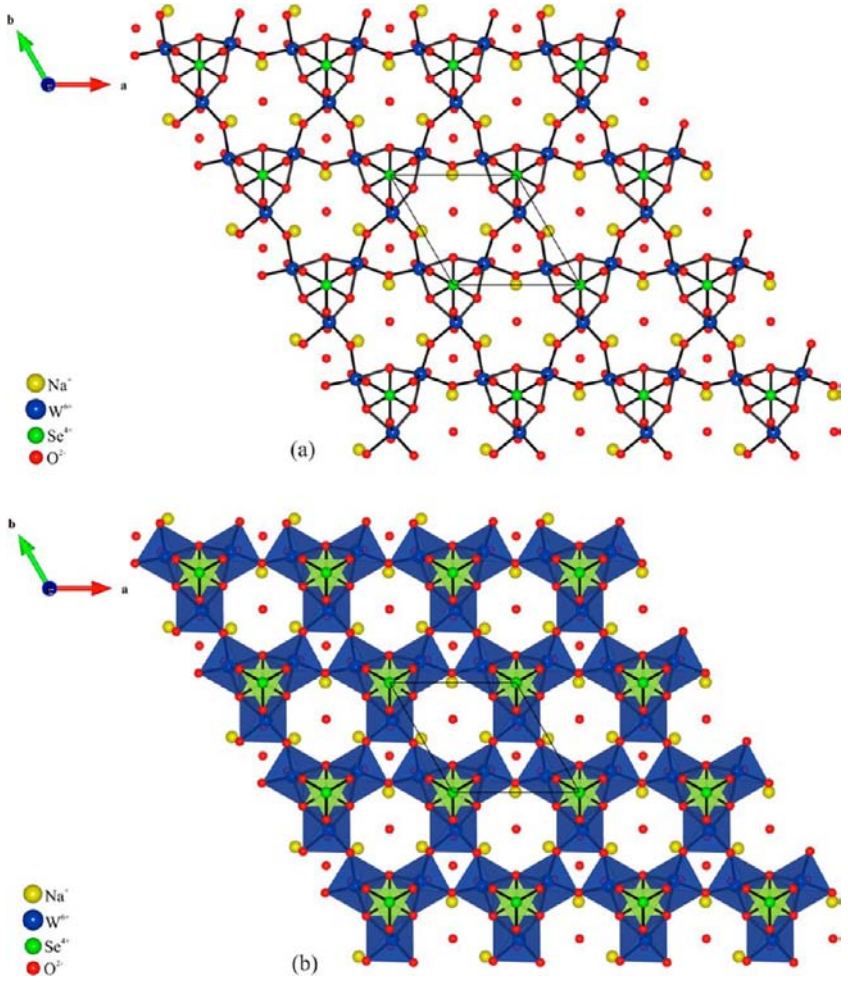

Figure 2. Ball-and-stick (top) and polyhedra (bottom) representations of $Na_2(WO_3)_3(SeO_3)\cdot 2H_2O$ in the *ab* plane. Spheres in the diagram are Na^+ cations (yellow), W^{6+} cations (blue), Se^{4+} cations (green), and O^{2-} anions (red). Isolated red spheres are the H_2O molecules.

all $Se(2)O_3$ polyhedra are oriented in the +*b*-axis direction. The "ribbons" are separated by Na^+ cations. In connectivity terms, the structure may be written as $[2(WO_{1/1}O_{5/2})^-2(WO_{1/1}O_{4/2}O_{1/3})^{2/3-}2(WO_{2/1}O_{3/2}O_{1/3})^{5/3-}(SeO_{2/1}O_{1/2})^-(SeO_{1/2}O_{2/3})^{5/3+}]^{6-}$ with charge balance maintained by six Na^+ cations. The W^{6+} cations are octahedrally coordinated to six O atoms. Of these W^{6+} cations, the W(1), W(3), W(5), and W(6) cations are subjected to a corner, C_4-type distortion with one "short" [1.702(9)−1.739(9) Å], four "normal" [1.830(9)−1.972(10) Å], and one "long" [2.122(11)−2.309(9) Å] W−O bonds, whereas the W(2) and W(4) cations are subjected to an edge, C_2-type distortion with two "short" [1.722(10)−1.753(10) Å], two "normal" [1.932(11)−1.943(11) Å], and two "long" [2.135(10)−2.366(10) Å] W−O bonds. All "short" W−O bonds are terminal, and as expected, the W^{6+} cations displace toward these terminal O atoms, whereas the "long" W−O bonds are connected to SeO_3 groups. The Se^{4+} cations are in trigonal-pyramidal environments, coordinated to three O atoms with Se−O bond distances in the range of 1.658(10)−1.765(10) Å. The Na^+ cations are in seven- and eight-coordinated environments, bonded to O atoms with Na−O bond distances in the range of 2.233(11)−3.098(11) Å. The experimental BVSs (vu)[75] for the Na^+, W^{6+}, and Se^{4+} cations and O^{2-} anions are in the ranges of 0.92−1.26, 6.00−6.24, 3.79−4.15, and 1.88−2.28 vu, respectively.

The relevant questions are the role of the H_2O molecules in the $Na_2(WO_3)_3(SeO_3)\cdot 2H_2O$ crystal structure and structural relationships between $Na_2(WO_3)_3(SeO_3)\cdot 2H_2O$ and $Na_6(W_6O_{19})(SeO_3)_2$. To answer this question, let us reexamine the crystal structures of compounds with the $B_2(MO_3)_3(AO_3)$ chemical formula (B = Ag^+, K^+, NH_4^+, Rb^+, Cs^+, and Tl^+; M = Mo^{6+} and W^{6+}; A = Se^{4+} and Te^{4+})[56,76−80] with respect to B cation sizes (see Table S3 in the Supporting Information). Except $Ag_2(MoO_3)_3(SeO_3)$ and $K_2(WO_3)_3(TeO_3)$, all other compounds exhibit HTO layers capped on one side by the AO_3 polyhedra (class 2 HTO layer). To examine the role of B cations, we plotted the HTO layer distances, that is, the oxide layer distances (see Figure 1a), and their cell parameters versus the B cation radius[81−83] for these class 2 HTO-layered materials. As seen in Figure 5, the blue circles are the oxide layer distances. For Tl^+, Rb^+, and Cs^+ compounds, the distances are linearly increasing with B cations (the blue line), consistent with Vegard's law.[84,85] For NH_4^+, the distance deviates from the blue line, with NH_4^+ points above the blue line. This deviation indicates new structural aspects occurring for $(NH_4)_2(MO_3)_3(AO_3)$ compounds. In fact, the N···O distances varying from 2.8(1) to 3.4(1) Å in $(NH_4)_2(MO_3)_3(AO_3)$ compounds indicate weak hydrogen bonding between NH_4^+ cations and oxide ligands of the HTO layers. Because NH_4^+ and K^+ cations have similar cation sizes (see Table S3 in the Supporting Information), we may expect that

dx.doi.org/10.1021/ic3026705 | *Inorg. Chem.* 2013, 52, 2637−2647

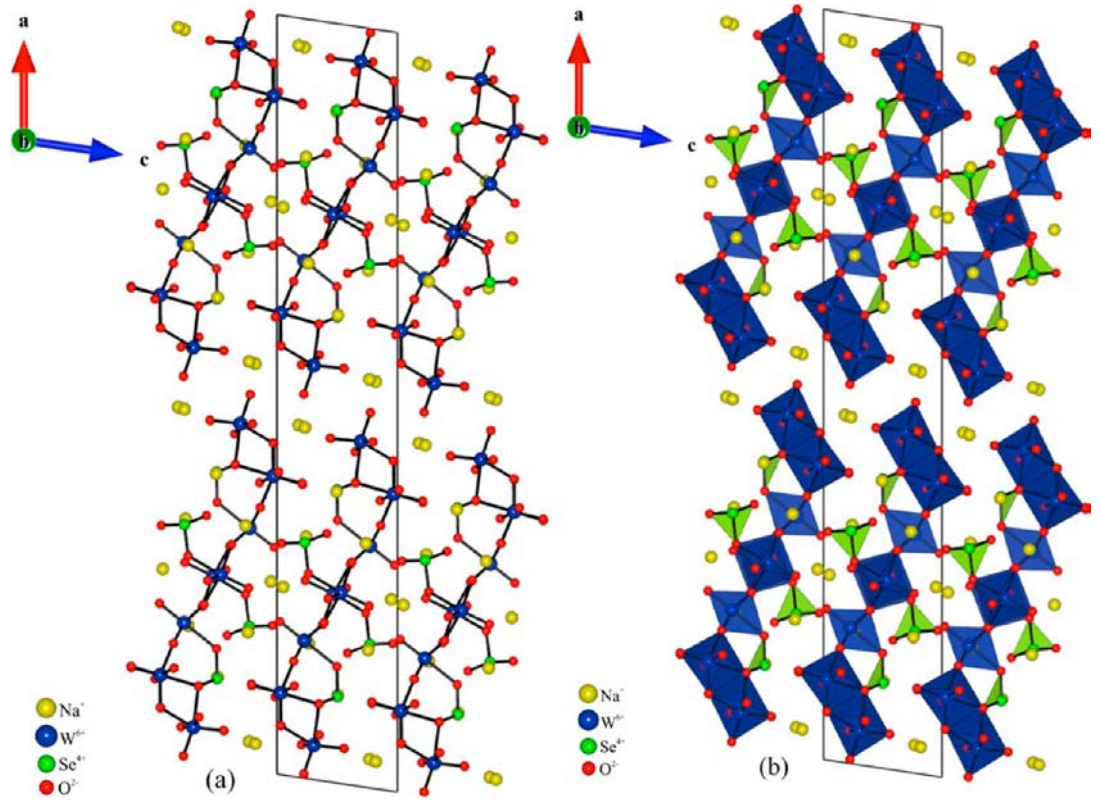

Figure 3. Ball-and-stick (left) and polyhedra (right) representations of $Na_6(W_6O_{19})(SeO_3)_2$ in the *ac* plane. Spheres in the diagram are Na^+ cations (yellow), W^{6+} cations (blue), Se^{4+} cations (green), and O^{2-} anions (red).

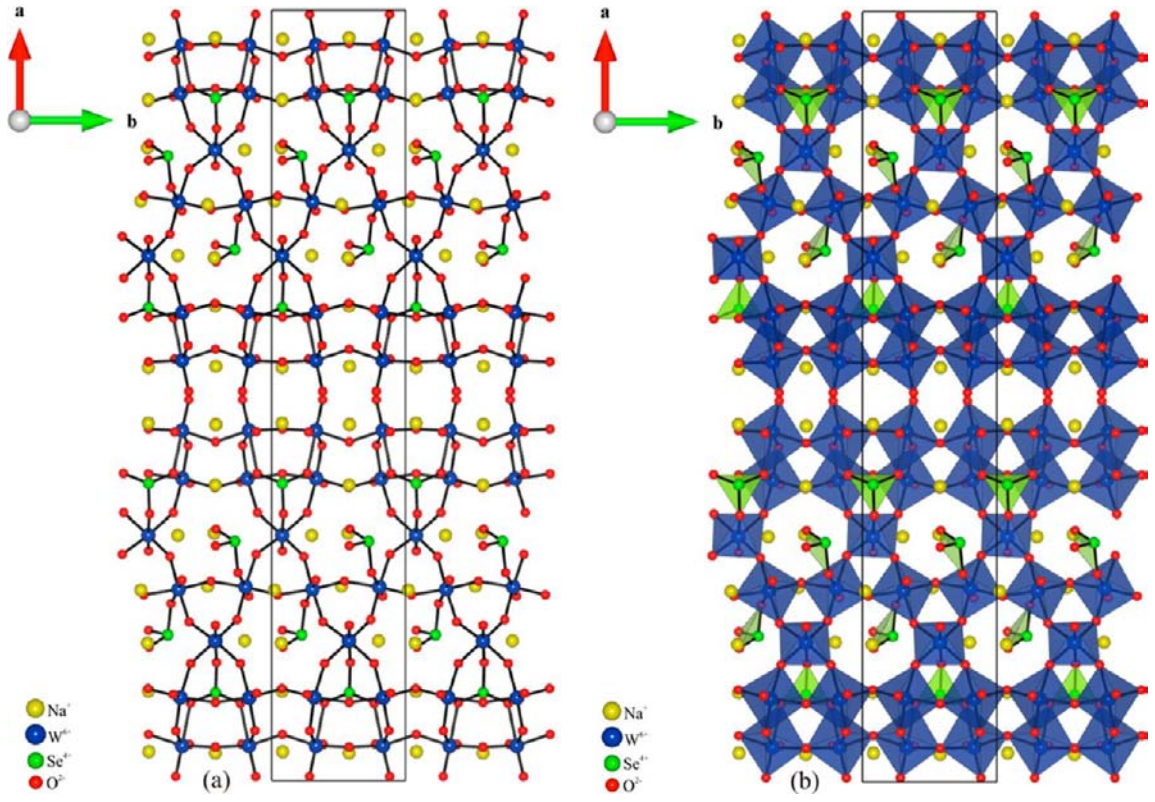

Figure 4. Ball-and-stick (left) and polyhedra (right) representations of $Na_6(W_6O_{19})(SeO_3)_2$ in the *ab* plane. Spheres in the diagram are Na^+ cations (yellow), W^{6+} cations (blue), Se^{4+} cations (green), and O^{2-} anions (red).

dx.doi.org/10.1021/ic3026705 | *Inorg. Chem.* 2013, 52, 2637−2647

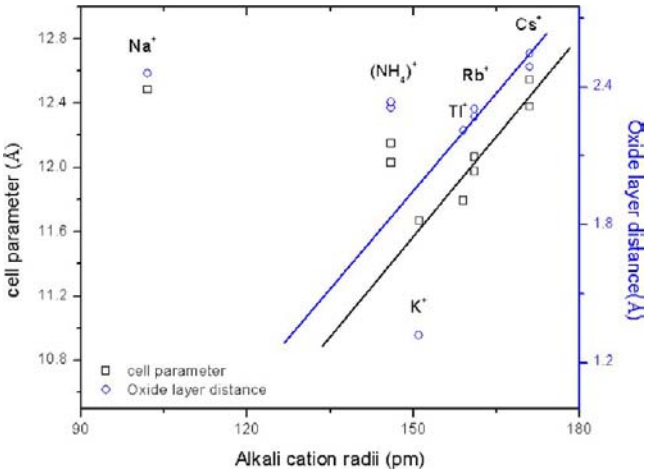

Figure 5. Plots of HTO layer distances and cell parameters of the polar HTO-layered materials versus the alkali cation radius.

$K_2(WO_3)_3(TeO_3)$ will also adopt the $(NH_4)_2(MO_3)_3(AO_3)$ structure if considering only cation size effects. However, $K_2(WO_3)_3(TeO_3)$ exhibits a CS structure with HTO layers connected by TeO_3 linkers. That was explained as the cation size effects because the K^+ cations are too small to fit in the space between the class 2 HTO layers, compared to bigger B cations like Tl^+, Rb^+, and Cs^+. Therefore, weak hydrogen bonding has a critical role in supporting the class 2 HTO-layered structure of $(NH_4)_2(MO_3)_3(AO_3)$. As mentioned earlier, the Na^+ cations are coordinated by seven O atoms in $Na_2(WO_3)_3(SeO_3)\cdot 2H_2O$, of which two are from the H_2O molecules with "short" Na−O bond distances [2.25(2)−2.47(4) Å]. The nearest O−O distances between the H_2O molecules and two adjacent HTO layers are in the range of 3.013(34)−3.380(40) Å. The O···O distances for weak hydrogen bonding in hydrated oxides are in the range of 2.59−3.48 Å.[86] That suggests that the H_2O molecules have weak hydrogen bonding to the HTO layers and ionic bonding to the Na^+ cations. To see the importance of the H_2O molecules in forming the $Na_2(WO_3)_3(SeO_3)\cdot 2H_2O$ structure, let us examine the $(Ag)_2(MoO_3)_3(SeO_3)$ structure because the Ag^+ and Na^+ cations are of similar ionic sizes. Without the H_2O molecules, we will expect that $(Ag)_2(MoO_3)_3(SeO_3)$ will exhibit a different crystal structure because the Ag^+ cation sizes are approximate to those of Na^+ cations but well smaller than those of K^+ cations (see Table S3 in the Supporting Information). In fact, $(Ag)_2(MoO_3)_3(SeO_3)$ crystallizes a CS-layered structure consisting of double-chain MoO_6 ribbons connected by SeO_3 polyhedra.[79] It is clear that weak hydrogen bonding between H_2O molecules and oxide ligands of the class 2 HTO layers in $Na_2(WO_3)_3(SeO_3)\cdot 2H_2O$ is essential to its polar structure. As expected, upon removal of the H_2O molecules, $Na_2(WO_3)_3(SeO_3)\cdot 2H_2O$ will lose its class 2 HTO-layered structure. In fact, $Na_6(W_6O_{19})(SeO_3)_2$ was formed with interesting structural aspects as described earlier. When the H_2O molecules were removed, the Na^+ cation size was too small to fit in the space between the class 2 HTO layers. The other aspect is that the Se−O bond lengths (~1.7 Å) are substantially shorter than the Te−O bond lengths (~1.9 Å). Therefore, the SeO_3 group cannot "serve" as an "interlayer" linker like the TeO_3 groups in connecting two adjacent HTO layers in $K_2(WO_3)_3(TeO_3)$. Thus, hydrogen bonding of the H_2O molecules together with ionic bonding of the Na^+ cations stabilize the class 2 HTO-layered structure of $Na_2(WO_3)_3(SeO_3)\cdot 2H_2O$.

Octahedral Distortion, ELF, Dipole Moments, BSI, and GII calculations. As mentioned earlier, $Na_2(WO_3)_3(SeO_3)\cdot 2H_2O$ and $Na_6(W_6O_{19})(SeO_3)_2$ contain the SOJT distorted cations, i.e., octahedrally coordinated d^0 transition-metal cations, W^{6+}, and lone-pair cations, Se^{4+}. We are able to quantify the magnitude of the displacement of the W^{6+} cations using the *SHAPE* program.[87] In the reported materials, the displacement magnitude is approximately 0.02−0.07 $Å^2$ for octahedrally C_4-type distorted W^{6+} cations and 0.11 $Å^2$ for octahedrally C_2-type distorted W^{6+} cations (see Table 4). These observations are consistent with those reported for the W^{6+} cations.[88]

With the lone-pair cations, ELF calculations were performed. As seen in Figure 6, violet lobelike ELF isosurfaces (η = 0.9) above the SeO_3 polyhedra are consistent with stereoactive lone pairs. In order to quantitatively examine the polarization magnitudes of the MO_6 and AO_3 polyhedra, the dipole moments were calculated using a method described earlier[89] and extended subsequently for lone-pair cations.[90] The calculated dipole moments for the WO_6 and SeO_3 polyhedra are 0.7−2.0 and 7.2−9.5 D, respectively. These values are consistent with those reported earlier.[56,90,91] With $Na_2(WO_3)_3(SeO_3)\cdot 2H_2O$, all dipole moments of the WO_6 and SeO_3 polyhedra are aligned in a parallel manner, and a large dipole moment of 64.8 D per unit cell is obtained along the *c*-axis direction, consistent with the polar axis direction of the crystal class, 3m.[92] For $Na_6(W_6O_{19})(SeO_3)_2$, the dipole moments of the WO_6 and $Se(1)O_3$ polyhedra are aligned in an antiparallel manner, whereas the dipole moments of the $Se(2)O_3$ polyhedra are all aligned in a parallel manner along the *b*-axis direction, resulting in a dipole moment of 34.4 D per unit cell along the *b*-axis direction, consistent with the polar axis direction of the crystal class, 2.[92]

In order to better understand the influence of the polar WO_6 and SeO_3 polyhedra on the structures of the reported materials, bond strain and global instability indices, BSI and GII, respectively, were calculated.[75,93,94] The BSI and GII indices are indicative of electronic- and lattice-induced strains, respectively. Values greater than 0.05 vu indicate that the structures are strained. Water O atoms [O(5) and O(6)] are not counted in the construction of a bond graph for $Na_2(WO_3)_3(SeO_3)\cdot 2H_2O$, and BVS calculations are scaled according partial occupancy of the Na^+ cations. For the

Table 3. BVSs, BSI, GII, and SHG Efficiencies (×α-SiO_2), Piezoelectric Responses, d_{33} (pm/V), Pyroelectric Coefficients at 60 °C, P_T ($\mu C/m^2\cdot K$), and Maximum Polarization, P_m ($\mu C/m^2$) for $Na_2(WO_3)_3(SeO_3)\cdot 2H_2O$ and $Na_6(W_6O_{19})(SeO_3)_2$

	BVS						functional properties		
compound	Na^+	W^{6+}	Se^{4+}	BSI	GII	SHG	d_{33}	P_T	P_m
$Na_2(WO_3)_3(SeO_3)\cdot 2H_2O$	1.16	6.17	3.96	0.23	0.07	450	23	−0.41	0.025
$Na_6(W_6O_{19})(SeO_3)_2$	0.92−1.25	6.00−6.18	3.79−4.15	0.16	0.13	20	12	−1.10	0.085

dx.doi.org/10.1021/ic3026705 | *Inorg. Chem.* 2013, 52, 2637−2647

Table 4. Distortion Magnitudes of WO_6 Octahedra and Dipole Moments of WO_6 and SeO_3 Polyhedra in $Na_2(WO_3)_3(SeO_3)\cdot 2H_2O$ and $Na_6(W_6O_{19})(SeO_3)_2$

compound		polyhedra dipole moment (D)			MO_6 distortion magnitude (Å^2)
$Na_2(WO_3)_3(SeO_3)\cdot 2H_2O$	WO_6	1.9	SeO_3	7.4	0.05
$Na_6(W_6O_{19})(SeO_3)_2$	$W(1)O_6$	1.5	$Se(1)O_3$	7.2	0.07
	$W(2)O_6$	1.4	$Se(2)O_3$	9.3	0.11
	$W(3)O_6$	1.8			0.07
	$W(4)O_6$	1.8			0.11
	$W(5)O_6$	0.7			0.05
	$W(6)O_6$	1.3			0.02

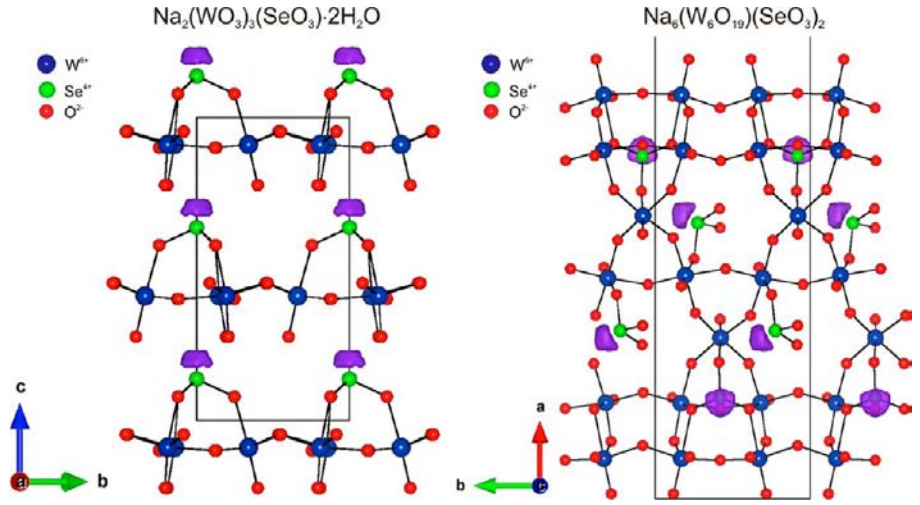

Figure 6. Ball-and-stick representations of (a) $Na_2(WO_3)_3(SeO_3)\cdot 2H_2O$ in the *bc* plane and (b) a half unit cell of $Na_6(W_6O_{19})(SeO_3)_2$ in the *ab* plane. ELF plots with $\eta = 0.9$ are also shown. The lobelike isosurfaces near the top of the SeO_3 polyhedra are consistent with stereoactive lone pairs on the Se^{4+} cations. The H_2O molecules in $Na_2(WO_3)_3(SeO_3)\cdot 2H_2O$ and the Na^+ cations have been removed for clarity.

reported materials, the BSI and GII values are greater than 0.05 vu (see Table 3). This is not surprising given the occurrence of asymmetric polyhedra. As seen in Table 3, the BSI values are 0.23 and 0.16 vu for $Na_2(WO_3)_3(SeO_3)\cdot 2H_2O$ and $Na_6(W_6O_{19})(SeO_3)_2$, respectively. The BSI values for $Na_2(WO_3)_3(SeO_3)\cdot 2H_2O$ are relatively larger than other class 2 HTO-layered materials (0.11–0.15 vu).[56] The larger BSI values are attributable to hydrogen bonding between polyhedra of the SOJT cations and H_2O molecules. Because no hydrogen bonding is present in $Na_6(W_6O_{19})(SeO_3)_2$, the BSI decreases but is still large because the SOJT distorted cations experienced two types of octahedral distortions, i.e., C_2- and C_4-type distortions with a variety of distortion magnitudes (0.02–0.11 Å^2). The GII indices are 0.11 and 0.13 vu for $Na_2(WO_3)_3(SeO_3)\cdot 2H_2O$ and $Na_6(W_6O_{19})(SeO_3)_2$, respectively. BSI > GII for both materials suggests that the structural strains are electronically induced; i.e., bond distances of SOJT cations are mainly determined by electronic SOJT distortions.

IR Spectroscopy. As described in the measurement procedure, $Na_2(WO_3)_3(SeO_3)\cdot 2H_2O$ and $Na_6(W_6O_{19})(SeO_3)_2$ powders were heated at 150 °C for 1 week to remove absorbed moisture before IR measurements. The IR spectrum of $Na_2(WO_3)_3(SeO_3)\cdot 2H_2O$ showed a broad absorption peak at 3550 cm^{-1} attributable to O–H stretching vibrations and a sharp strong absorption peak at 1619 cm^{-1} attributable to H–O–H bending vibrations.[95] The existence of these peaks therefore clearly confirms the presence of the H_2O molecules in the crystal structure of $Na_2(WO_3)_3(SeO_3)\cdot 2H_2O$. For the IR spectrum of $Na_6(W_6O_{19})(SeO_3)_2$, there are no absorption peaks in the range of 1000–4000 cm^{-1}. Below 1000 cm^{-1}, both materials showed W–O stretching vibrations in the range of 814–977 cm^{-1}, Se–O stretching vibrations in the range of 613–760 cm^{-1}, and Se–O–Se(W) bending vibrations below 600 cm^{-1}. These assignments are in good agreement with the literature.[96–98] The IR spectra and assignments were deposited in the Supporting Information (see Figure S2).

UV–Vis Diffuse-Reflectance Spectroscopy. Reflectance spectra of $Na_2(WO_3)_3(SeO_3)\cdot 2H_2O$ and $Na_6(W_6O_{19})(SeO_3)_2$ were converted to absorbance using the Kubelka–Munk function:[63,64]

$$F(R) = (1 - R)^2/2R = K/S$$

where R, K, and S represent reflectance, absorption, and scattering, respectively. In a $F(R)$ versus E (eV) plot, extrapolating the linear part of the rising curve to zero provides onset absorption values of 3.2 and 2.9 eV for $Na_2(WO_3)_3(SeO_3)\cdot 2H_2O$ and $Na_6(W_6O_{19})(SeO_3)_2$, respectively. These values are consistent with the transparency of the materials in the visible wavelength range. The band gap may be explained by the ligand-to-metal charge transfer from the O 2p band (highest occupied molecular orbital) to the lowest unoccupied molecular orbital band consisting of mainly metal W 5d and Se 4sp states. The UV–vis diffuse-reflectance spectra for the reported compounds were deposited in the Supporting Information (see Figure S3).

Thermal Analysis. The thermal stability of $Na_2(WO_3)_3(SeO_3)\cdot 2H_2O$ and $Na_6(W_6O_{19})(SeO_3)_2$ was investigated through TGA and DTA, respectively. The TGA and DTA data of $Na_2(WO_3)_3(SeO_3)\cdot 2H_2O$ showed that the oxide

dx.doi.org/10.1021/ic3026705 | *Inorg. Chem.* 2013, 52, 2637–2647

experienced two weight loss steps in the temperature range of 25−700 °C. The first weight loss (3.8%) occurs in the temperature range of 200−300 °C, where the H_2O molecules were released out of the material (calculated weight percentage of the H_2O molecules is 4.0%). The second weight loss (11.9%) happened above 450 °C, where the material released SeO_2 (calculated weight percentage of SeO_2 is 12.2%). The PXRD analysis showed $Na_2(WO_3)_3(SeO_3)\cdot 2H_2O$ finally decomposed to a mixture of $Na_2W_2O_7$ and $Na_2W_4O_{13}$, as described by the following equation:

$$2Na_2(WO_3)_3(SeO_3)\cdot 2H_2O \xrightarrow{\Delta} Na_2W_2O_7 + Na_2W_4O_{13} + 2SeO_2 + 4H_2O$$

The TGA and DTA data of $Na_6(W_6O_{19})(SeO_3)_2$ showed that the oxide experienced two consecutive weight loss steps in the temperature range of 450−700 °C. The total experimental weight loss of 12.3% is in agreement with the fact that $Na_6(W_6O_{19})(SeO_3)_2$ lost two SeO_2 molecules at high temperature (calculated weight percentage of SeO_2 is 12.3%). The observation of two consecutive weight losses during the thermal analysis of $Na_6(W_6O_{19})(SeO_3)_2$ reflects two different SeO_3 bonding groups: one capped on triangular holes and one single-bonded to the $W(6)O_6$ "single chain". The PXRD analysis showed that $Na_6(W_6O_{19})(SeO_3)_2$ finally decomposed to $Na_2W_2O_7$ as described by the following equation:

$$Na_6(W_6O_{19})(SeO_3)_2 \xrightarrow{\Delta} 3Na_2W_2O_7 + 2SeO_2$$

The TGA and DTA data and PXRD patterns of the residuals are deposited in the Supporting Information (see Figures S5 and S6).

SHG. Powder SHG measurements in the particle size range of 25−120 μm indicated that $Na_2(WO_3)_3(SeO_3)\cdot 2H_2O$ and $Na_6(W_6O_{19})(SeO_3)_2$ were non-phase-matching materials (see Figure S7 in the Supporting Information). In the particle size range of 45−63 μm, $Na_2(WO_3)_3(SeO_3)\cdot 2H_2O$ has a strong SHG efficiency of 450× α-SiO_2, which is similar to the magnitudes of the SHG efficiencies of other class 2 HTO-layered materials,[56,76,78,80,99] whereas $Na_6(W_6O_{19})(SeO_3)_2$ exhibits a weak SHG efficiency of 20× α-SiO_2. As defined by Kurtz and Perry,[65] $Na_2(WO_3)_3(SeO_3)\cdot 2H_2O$ falls into the class C of SHG materials and $Na_6(W_6O_{19})(SeO_3)_2$ belongs to the class D of SHG materials. The average NLO susceptibilities, $\langle d_{eff}\rangle_{exp}$, for $Na_2(WO_3)_3(SeO_3)\cdot 2H_2O$ and $Na_6(W_6O_{19})(SeO_3)_2$ can be estimated to be ~11.7 and 2.5 pm/V, respectively. The strong SHG efficiency of $Na_2(WO_3)_3(SeO_3)\cdot 2H_2O$ can be understood because all stereoactive lone pairs of the SeO_3 groups are aligned in a parallel manner toward the *c*-axis direction. For $Na_6(W_6O_{19})(SeO_3)_2$, because of the internal 2-fold rotation of the "ribbon" about the $W(6)O_6$ "single chain", all dipole moments of the $W(x)O_6$ (x = 1−5) and $Se(1)O_3$ polyhedra cancel. Only the dipole moments of the $W(6)O_6$ and $Se(2)O_3$ polyhedra, with a net magnitude of 34.4 D along the *b*-axis direction, remain. Thus, it is expected that the SHG efficiency of $Na_6(W_6O_{19})(SeO_3)_2$ will be weaker than that of $Na_2(WO_3)_3(SeO_3)\cdot 2H_2O$. In fact, $Na_6(W_6O_{19})(SeO_3)_2$ was experimentally observed as having a weaker SHG efficiency than $Na_2(WO_3)_3(SeO_3)\cdot 2H_2O$.

Piezoelectricity Measurements. Converse piezoelectric measurements were performed on $Na_2(WO_3)_3(SeO_3)\cdot 2H_2O$ and $Na_6(W_6O_{19})(SeO_3)_2$ pellets at room temperature. A voltage of 1000 V at 100 Hz was applied for $Na_2(WO_3)_3(SeO_3)\cdot 2H_2O$ pellets and a voltage of 2000 V at 100 Hz was applied for $Na_6(W_6O_{19})(SeO_3)_2$. The d_{33} piezoelectric charge constants,[66] which are defined as the ratios between the strain produced and electrical voltage applied, for $Na_2(WO_3)_3(SeO_3)\cdot 2H_2O$ and $Na_6(W_6O_{19})(SeO_3)_2$ were estimated to be 23 and 12 pm/V, respectively. These charge constants are comparable to class 2 HTO-layered materials, $A_2(MoO_3)_3(SeO_3)$ (A = Rb^+ and Tl^+; d_{33} = 9−11 pm/V),[56] or $Na_2TeW_2O_9$ (d_{33} = 13.9 pm/V).[100] The piezoelectric data were deposited in the Supporting Information (see Figure S8).

Polarization Measurements. $Na_2(WO_3)_3(SeO_3)\cdot 2H_2O$ ($P3_1c$) and $Na_6(W_6O_{19})(SeO_3)_2$ ($C2$) are polar materials, and a macroscopic dipole moment is observed. The macroscopic polarity suggests the possibility for ferroelectric behavior. Ferroelectric hysteresis measurements were performed on the pressed pellets, and polarization loops were observed. In addition, these loops did appear to exhibit a frequency dependence (see Figure S9 in the Supporting Information). However, these loops are not attributable to ferroelectric hysteresis; i.e., the reported materials are not ferroelectric, and the macroscopic polarization cannot be reversed in the presence of an external electric field. It has been demonstrated that these types of loops have been erroneously attributed to ferroelectric behavior.[101] With the reported materials, it is important to understand why the materials, although polar, are not ferroelectric. As stated earlier, for ferroelectric behavior to occur, the macroscopic polarization must be switchable in the presence of an external electric field. This implies that the local moments must also be reversed. In $Na_2(WO_3)_3(SeO_3)\cdot 2H_2O$ and $Na_6(W_6O_{19})(SeO_3)_2$, the dipole moments are associated with distorted WO_6 and asymmetric SeO_3 polyhedra. We have already shown that the energy barrier to inversion of a SeO_3 trigonal pyramid is ~5.3 eV,[33] which is substantially larger than that observed in ferroelectric $BaTiO_3$ (1.8×10^{-2} eV) and $PbTiO_3$ (2.0×10^{-1} eV).[102] Thus, it is energetically unfavorable for polarization reversal to occur. Therefore, $Na_2(WO_3)_3(SeO_3)\cdot 2H_2O$ and $Na_6(W_6O_{19})(SeO_3)_2$ are pyroelectric and not ferroelectric.

Pyroelectric measurements were performed by measuring the spontaneous polarization (P_S) as a function of the temperature. The values of the pyroelectric coefficient, which is defined as dP/dT,[66] for $Na_2(WO_3)_3(SeO_3)\cdot 2H_2O$ and $Na_6(W_6O_{19})(SeO_3)_2$ at 60 °C are −0.41 and −1.10 $\mu C/m^2\cdot K$, respectively. The magnitudes of these pyroelectric coefficients are similar to other class 2 HTO-layered materials, $A_2(MoO_3)_3(SeO_3)$ (A = Rb^+ and Tl^+; −1.1 to −2.1 $\mu C/m^2\cdot K$).[56] The polarization data were deposited in the Supporting Information (see Figure S9).

CONCLUSION

Two new sodium tungsten selenites, $Na_2(WO_3)_3(SeO_3)\cdot 2H_2O$ ($P3_1c$) and $Na_6(W_6O_{19})(SeO_3)_2$ ($C2$), have been synthesized and characterized. $Na_2(WO_3)_3(SeO_3)\cdot 2H_2O$ exhibits a class 2 HTO-layered structure (i.e., the SeO_3 groups "cap" on one side of the HTO layers), and $Na_6(W_6O_{19})(SeO_3)_2$ exhibits a one-dimensional complex "ribbon" structure. $Na_2(WO_3)_3(SeO_3)\cdot 2H_2O$ exhibits a strong SHG efficiency of 450× α-SiO_2, and $Na_6(W_6O_{19})(SeO_3)_2$ shows a weak SHG efficiency of 20× α-SiO_2. Finally, the polarization measurements indicate that both oxides are pyroelectric and not ferroelectric materials.

dx.doi.org/10.1021/ic3026705 | Inorg. Chem. 2013, 52, 2637−2647

■ ASSOCIATED CONTENT

Supporting Information

X-ray crystallographic files in CIF format, experimental and calculated PXRD patterns, IR and UV−vis spectra, thermogravimetric and differential thermal analysis diagrams, SHG behavior, piezoelectric curves, polarization-electric loops, and BVSs for $Na_2(WO_3)_3(SeO_3)\cdot 2H_2O$ and $Na_6(W_6O_{19})(SeO_3)_2$. This material is available free of charge via the Internet at http://pubs.acs.org.

■ AUTHOR INFORMATION

Corresponding Author

*E-mail: psh@uh.edu.

Notes

The authors declare no competing financial interest.

■ ACKNOWLEDGMENTS

We thank the Robert A. Welch Foundation (Grant E-1457) for support. S.D.N. thanks the Vietnam Government for an opportunity to study at the University of Houston.

■ REFERENCES

(1) Boyd, R. W. *Nonlinear Optimization*, 3rd ed.; Academic Press: New York, 2008.
(2) Cady, W. G. *Piezoelectricity; an Introduction to the Theory and Applications of Electromechanical Phenomena in Crystals*, revised ed.; Dover: New York, 1964.
(3) Capper, P. *Bulk Crystal Growth of Electronic, Optical and Optoelectronic Materials*; John Wiley & Sons, Inc.: New York, 2005.
(4) Jaffe, B.; Cook, W. R. *Piezoelectric ceramics*; Academic Press: New York, 1971.
(5) Jona, F.; Shirane, G. *Ferroelectric Crystals*; Pergamon Press: Oxford, U.K., 1961.
(6) Lang, S. B. *Sourcebook of Pyroelectricity*; Gordon and Breach: New York, 1974.
(7) Lang, S. B.; Das-Gupta, D. K. *Pyroelectricity: fundamentals and applications*; Academic Press: New York, 2001; Vol. *4*.
(8) Lines, M. E.; Glass, A. M. *Principles and Applications of Ferroelectrics and Related Materials*; Oxford University Press: Oxford, U.K., 1991.
(9) Eaton, D. F. *Science* **1991**, *253*, 281.
(10) Bosshard, C.; Hulliger, J.; Florsheimer, M. *Organic Nonlinear Optical Materials*; CRC Press: Boca Raton, FL, 2001.
(11) Chen, C.; Wu, Y.; Li, R. *Int. Rev. Phys. Chem.* **1989**, *8*, 65.
(12) Chen, C. T. *Acta Phys. Sin.* **1976**, *25*, 146.
(13) Chen, C. T. *Acta Phys. Sin.* **1977**, *26*, 124.
(14) Chen, C. T. *Acta Phys. Sin.* **1979**, *22*, 756.
(15) Zou, G.; Ye, N.; Huang, L.; Lin, X. *J. Am. Chem. Soc.* **2011**, *133*, 20001.
(16) Heier, K. R.; Norquist, A. J.; Halasyamani, P. S.; Duarte, A.; Stern, C. L.; Poeppelmeier, K. R. *Inorg. Chem.* **1999**, *38*, 762.
(17) Welk, M. E.; Norquist, A. J.; Stern, C. L.; Poeppelmeier, K. R. *Inorg. Chem.* **2000**, *39*, 3946.
(18) Izumi, H. K.; Kirsch, J. E.; Stern, C. L.; Poeppelmeier, K. R. *Inorg. Chem.* **2005**, *44*, 884.
(19) Marvel, M. R.; Lesage, J.; Baek, J.; Halasyamani, P. S.; Stern, C. L.; Poeppelmeier, K. R. *J. Am. Chem. Soc.* **2007**, *129*, 13963.
(20) Donakowski, M. D.; Gautier, R.; Yeon, J.; Moore, D. T.; Nino, J. C.; Halasyamani, P. S.; Poeppelmeier, K. R. *J. Am. Chem. Soc.* **2012**, *134*, 7679.
(21) Bader, R. F. W. *Mol. Phys.* **1960**, *3*, 137.
(22) Bader, R. F. W. *Can. J. Chem.* **1962**, *40*, 1164.
(23) Goodenough, J. B. *Annu. Rev. Mater. Sci.* **1998**, *28*, 1.
(24) Kunz, M.; Brown, I. D. *J. Solid State Chem.* **1995**, *115*, 395.
(25) Opik, U.; Pryce, M. H. L. *Proc. R. Soc. London, Ser. A* **1957**, *238*, 425.
(26) Pearson, R. G. *J. Mol. Struct.: THEOCHEM* **1983**, *103*, 25.
(27) Pearson, R. G. *J. Am. Chem. Soc.* **1969**, *91*, 4947.
(28) Halasyamani, P. S.; Poeppelmeier, K. R. *Chem. Mater.* **1998**, *10*, 2753.
(29) Ra, H.-S.; Ok, K. M.; Halasyamani, P. S. *J. Am. Chem. Soc.* **2003**, *125*, 7764.
(30) Ok, K. M.; Halasyamani, P. S. *Angew. Chem., Int. Ed.* **2004**, *43*, 5489.
(31) Chi, E. O.; Ok, K. M.; Porter, Y.; Halasyamani, P. S. *Chem. Mater.* **2006**, *18*, 2070.
(32) Sivakumar, T.; Chang, H. Y.; Baek, J.; Halasyamani, P. S. *Chem. Mater.* **2007**, *19*, 4710.
(33) Kim, S.-H.; Yeon, J.; Halasyamani, P. S. *Chem. Mater.* **2009**, *21*, 5335.
(34) Chang, H. Y.; Kim, S.-H.; Ok, K. M.; Halasyamani, P. S. *Chem. Mater.* **2009**, *21*, 1654.
(35) Yeon, J.; Kim, S.-H.; Halasyamani, P. S. *Inorg. Chem.* **2010**, *49*, 6986.
(36) Kong, F.; Huang, S.-P.; Sun, Z.-M.; Mao, J.-G.; Cheng, W.-D. *J. Am. Chem. Soc.* **2006**, *128*, 7750.
(37) Sun, C.-F.; Hu, C.-L.; Xu, X.; Ling, J.-B.; Hu, T.; Kong, F.; Long, X.-F.; Mao, J.-G. *J. Am. Chem. Soc.* **2009**, *131*, 9486.
(38) Yang, B.-P.; Hu, C.-L.; Xu, X.; Sun, C.-F.; Zhang, J.-H.; Mao, J.-G. *Chem. Mater.* **2010**, *22*, 1545.
(39) Hernàndez, E.; Mas, M.; Molins, E.; Rovira, C.; Veciana, J. *Angew. Chem., Int. Ed. Engl.* **1993**, *32*, 882.
(40) Moulton, B.; Zaworotko, M. J. *Chem. Rev.* **2001**, *101*, 1629.
(41) Brammer, L. *Chem. Soc. Rev.* **2004**, *33*, 476.
(42) Subramanian, S.; Zaworotko, M. J. *Coord. Chem. Rev.* **1994**, *137*, 357.
(43) Chang, Y.-F.; Lu, Z.-Y.; An, L.-J.; Zhang, J.-P. *J. Phys. Chem. C* **2011**, *116*, 1195.
(44) Etter, M. C.; Frankenbach, G. M.; Adsmond, D. A. *Mol. Cryst. Liq. Cryst.* **1990**, *187*, 25.
(45) Debrus, S.; Ratajczak, H.; Venturini, J.; Pinçon, N.; Baran, J.; Barycki, J.; Glowiak, T.; Pietraszko, A. *Synth. Met.* **2002**, *127*, 99.
(46) Zhang, F.; Li, K.; Xue, D.; Pan, S. *Rev. Adv. Sci. Eng.* **2012**, *1*, 75.
(47) Chang, H.-Y.; Kim, S.-H.; Ok, K. M.; Halasyamani, P. S. *J. Am. Chem. Soc.* **2009**, *131*, 6865.
(48) Yeon, J.; Kim, S.-H.; Hayward, M. A.; Halasyamani, P. S. *Inorg. Chem.* **2011**, *50*, 8663.
(49) Oh, S.-J.; Lee, D. W.; Ok, K. M. *Inorg. Chem.* **2012**, *51*, 5393.
(50) Fry, A. M.; Seibel, H. A.; Lokuhewa, I. N.; Woodward, P. M. *J. Am. Chem. Soc.* **2011**, *134*, 2621.
(51) Darriet, J.; Guillaume, G.; Galy, J. *C. R. Acad. Sci., Ser. C* **1969**, *269*, 23.
(52) Darriet, J.; Guillaume, G.; Wilhelmi, K. A.; Galy, J. *Acta Chem. Scand.* **1972**, *26*, 59.
(53) Vidyavathy, B.; Vidyasagar, K. *Inorg. Chem.* **1999**, *38*, 5809.
(54) Goodey, J.; Broussard, J.; Halasyamani, P. S. *Chem. Mater.* **2002**, *14*, 3174.
(55) Porter, Y.; Halasyamani, P. S. *J. Solid State Chem.* **2003**, *174*, 441.
(56) Chang, H. Y.; Kim, S. W.; Halasyamani, P. S. *Chem. Mater.* **2010**, *22*, 3241.
(57) *SAINT, Program for Area Detector Absorption Correction*, version 4.05; Siemens Analytical X-ray Systems, Inc.: Madison, WI, 1995.
(58) North, A. C. T.; Phillips, D. C.; Mathews, F. S. *Acta Crystallogr.* **1968**, *24*, 351.
(59) Sheldrick, G. M. *SHELXL-97—A program for crystal structure refinement*; University of Goettingen: Goettingen, Germany, 1997.
(60) Sheldrick, G. M. *SHELXS-97—A program for automatic solution of crystal structures*; University of Goettingen: Goettingen, Germany, 1997.
(61) Farrugia, L. J. *J. Appl. Crystallogr.* **1999**, *32*, 837.
(62) Flack, H. *Acta Crystallogr.* **1983**, *39*, 876.
(63) Kubelka, P.; Munk, F. *Z. Tech. Phys.* **1931**, *12*, 593.
(64) Tauc, J. *Mater. Res. Bull.* **1970**, *5*, 721.
(65) Kurtz, S. K.; Perry, T. T. *J. Appl. Phys.* **1968**, *39*, 3798.

(66) Ok, K. M.; Chi, E. O.; Halasyamani, P. S. *Chem. Soc. Rev.* **2006**, *35*, 710.
(67) Becke, A. D.; Edgecombe, K. E. *J. Chem. Phys.* **1990**, *92*, 5397.
(68) Silvi, B.; Savin, A. *Nature* **1994**, *371*, 683.
(69) Giannozzi, P. *J. Phys: Condens. Matter* **2009**, *21*, 395502.
(70) Perdew, J. P.; Burke, K.; Ernzerhof, M. *Phys. Rev. Lett.* **1996**, *77*, 3865.
(71) Fuchs, M.; Scheffler, M. *Comput. Phys. Commun.* **1999**, *119*, 67.
(72) Walkingshaw, A. D.; Spaldin, N. A.; Artacho, E. *Phys. Rev. B: Condens. Matter* **2004**, *70*, 165110.
(73) Monkhorst, H. J.; Pack, J. D. *Phys. Rev. B* **1976**, *13*, 5188.
(74) Momma, K.; Izumi, F. *J. Appl. Crystallogr.* **2008**, *41*, 653.
(75) Brown, I. D. *The Chemical Bond in Inorganic Chemistry: The Bond Valence Model*, 1st ed.; Oxford University Press: Oxford, U.K., 2002.
(76) Harrison, W. T. A.; Dussack, L. L.; Jacobson, A. J. *Inorg. Chem.* **1994**, *33*, 6043.
(77) Vidyavathy, B.; Vidyasagar, K. *Inorg. Chem.* **1998**, *37*, 4764.
(78) Harrison, W. T. A.; Dussack, L. L.; Vogt, T.; Jacobson, A. J. *J. Solid State Chem.* **1995**, *120*, 112.
(79) Ling, J.; Albrecht-Schmitt, T. E. *J. Solid State Chem.* **2007**, *180*, 1601.
(80) Dussack, L. L.; Harrison, W. T. A.; Jacobson, A. J. *Mater. Res. Bull.* **1996**, *31*, 249.
(81) Shannon, R. D.; Prewitt, C. T. *Acta Crystallogr.* **1969**, *25*, 925.
(82) Shannon, R. D.; Prewitt, C. T. *Acta Crystallogr.* **1970**, *26*, 1046.
(83) Shannon, R. *Acta Crystallogr.* **1976**, *32*, 751.
(84) Denton, A. R.; Ashcroft, N. W. *Phys. Rev. A* **1991**, *43*, 3161.
(85) Vegard, L. *Z. Phys. A: Hadrons Nucl.* **1921**, *5*, 17.
(86) Libowitzky, E. *Monats.* **1999**, *130*, 1047.
(87) Llunell, M.; Casanova, D.; Cirera, J.; Bofill, J. M.; Alemany, P.; Alvarez, S.; Pinsky, M.; Avnir, D. *SHAPE Program*, version 2.0; University of Barcelona: Barcelona, Spain: 2003.
(88) Ok, K. M.; Halasyamani, P. S.; Casanova, D.; Llunell, M.; Alemany, P.; Alvarez, S. *Chem. Mater.* **2006**, *18*, 3176.
(89) Maggard, P. A.; Nault, T. S.; Stern, C. L.; Poeppelmeier, K. R. *J. Solid State Chem.* **2003**, *175*, 27.
(90) Ok, K. M.; Halasyamani, P. S. *J. Solid State Chem.* **2006**, *179*, 1345.
(91) Chang, H. Y.; Ok, K. M.; Kim, J. H.; Halasyamani, P. S.; Stoltzfus, M.; Woodward, P. *Inorg. Chem.* **2007**, *46*, 7005.
(92) *International Tables for Crystallography, Vol. A, Space Group Symmetry*; Hahn, T., Ed.; Kluwer Academic: Dordrecht, Holland, 2006; Vol. *A*.
(93) Preiser, C.; Losel, J.; Brown, I. D.; Kunz, M.; Skowron, A. *Acta Crystallogr.* **1999**, *55*, 698.
(94) Salinas-Sanchez, A.; Garcia-Muñoz, J. L.; Rodriguez-Carvajal, J.; Saez-Puche, R.; Martinez, J. L. *J. Solid State Chem.* **1992**, *100*, 201.
(95) Falk, M. *Spectrochim. Acta, Part A* **1984**, *40A*, 43.
(96) Frechero, M. A.; Quinzani, O. V.; Pettigrosso, R. S.; Villar, M.; Montani, R. A. *J. Non-Cryst. Solids* **2007**, *353*, 2919.
(97) Harrison, W. T. A.; Dussack, L. L.; Jacobson, A. J. *J. Solid State Chem.* **1996**, *125*, 234.
(98) Kurilenko, L. N.; Serebryakova, N. V.; Saunin, E. I.; Gromov, V. V.; Sokolova, N. P. *Russ. Chem. Bull.* **1988**, *37*, 839.
(99) Goodey, J.; Ok, K. M.; Broussard, J.; Hofmann, C.; Escobedo, F. V.; Halasyamani, P. S. *J. Solid State Chem.* **2003**, *175*, 3.
(100) Zhang, W.; Li, F.; Kim, S.-H.; Halasyamani, P. S. *Cryst. Growth Des.* **2010**, *10*, 4091.
(101) Scott, J. F. *J. Phys.: Condens. Matter* **2008**, *20*, 021001.
(102) Cohen, R. E. *Nature* **1992**, *358*, 136.